

# Trichomes of Tobacco Excrete Zinc as Zinc-Substituted Calcium Carbonate and Other Zinc-Containing Compounds<sup>1[W]</sup>

Géraldine Sarret, Emiko Harada, Yong-Eui Choi\*, Marie-Pierre Isaure, Nicolas Geoffroy, Sirine Fakra, Matthew A. Marcus, Mandy Birschwilks, Stephan Clemens, and Alain Manceau

Environmental Geochemistry Group, Laboratoire de Géophysique Interne et Tectonophysique, University of Grenoble and Centre National de la Recherche Scientifique, 38041 Grenoble cedex 9, France (G.S., E.H., M.-P.I., N.G., A.M.); Division of Forest Resources, College of Forest Sciences, Kangwon National University, Chunchon 200-701, Kangwon-do, Korea (E.H., Y.-E.C.); Leibniz-Institut für Pflanzenbiochemie, 06120 Halle (Saale), Germany (E.H., M.B., S.C.); and Advanced Light Source, Berkeley Lab, MS 6-2100, Berkeley, California 94720 (S.F., M.A.M.)

Tobacco (*Nicotiana tabacum* L. cv Xanthi) plants were exposed to toxic levels of zinc (Zn). Zn exposure resulted in toxicity signs in plants, and these damages were partly reduced by a calcium (Ca) supplement. Confocal imaging of intracellular Zn using Zinquin showed that Zn was preferentially accumulated in trichomes. Exposure to Zn and Zn + Ca increased the trichome density and induced the production of Ca/Zn mineral grains on the head cells of trichomes. These grains were aggregates of submicrometer-sized crystals and poorly crystalline material and contained Ca as major element, along with subordinate amounts of Zn, manganese, potassium, chlorine, phosphorus, silicon, and magnesium. Micro x-ray diffraction revealed that the large majority of the grains were composed essentially of metal-substituted calcite (CaCO<sub>3</sub>). CaCO<sub>3</sub> polymorphs (aragonite and vaterite) and CaC<sub>2</sub>O<sub>4</sub> (Ca oxalate) mono- and dihydrate also were identified, either as an admixture to calcite or in separate grains. Some grains did not diffract, although they contained Ca, suggesting the presence of amorphous form of Ca. The presence of Zn-substituted calcite was confirmed by Zn K-edge micro-extended x-ray absorption fine structure spectroscopy. Zn bound to organic compounds and Zn-containing silica and phosphate were also identified by this technique. The proportion of Zn-substituted calcite relative to the other species increased with Ca exposure. The production of Zn-containing biogenic calcite and other Zn compounds through the trichomes is a novel mechanism involved in Zn detoxification. This study illustrates the potential of laterally resolved x-ray synchrotron radiation techniques to study biomineralization and metal homeostasis processes in plants.

Smoking of tobacco (*Nicotiana tabacum*) leaves is one of the principal routes of exposure to heavy metals. Metals contained in tobacco leaves originate from root uptake and transfer to the shoots and also from deposition of aerosol particles on the leaves (Fleisher and Parungo, 1974). Efforts have been made to minimize toxic metal contents in the leaves (Lugon-

Moulin et al., 2004). However, this is not the case for counterfeit tobacco products, which contain higher concentrations of metals than their genuine equivalents (Stephens et al., 2005). Besides its primary application for leaf production, tobacco is also a candidate for phytoextraction. Although this plant species is not a hyperaccumulator, it has several advantages, including a high biomass, moderate soil requirements, fast growth rate, and ease of harvesting. For this particular application, research is conducted with the aim of enhancing metal accumulation in the shoots (Song et al., 2003).

Little is known about the mechanisms of metals accumulation and detoxification in tobacco. The exposure of plants to high concentrations of metals generally induces a stress, whose visible symptoms include an inhibition of root elongation, a decrease in shoot growth, leaf chlorosis, and necrosis of the tissues. This stress is generated by the perturbation of cell metabolism by metals, mostly due to the inactivation of proteins by adventitious binding. Plants have developed various mechanisms to tolerate heavy metals in their tissues (Küpper and Kroneck, 2005). One of the most important mechanisms is the sequestration of heavy metals in specific subcellular compartments of particular tissues, whose nature depends on the plant

<sup>1</sup> This work was supported by the BioGreen 21 Program, Rural Development Administration, in Korea. The operations of the Advanced Light Source at Lawrence Berkeley National Laboratory are supported by the Director, Office of Science, Office of Basic Energy Sciences, Materials Sciences Division, of the U.S. Department of Energy (contract no. DEAC03-76SF00098). E.H. is the recipient of fellowships from the BioGreen 21 program, the International Human Frontier Science Program Organization, and the Alexander von Humboldt Foundation.

\* Corresponding author; e-mail yechoi@kangwon.ac.kr; fax 82-33-252-8310.

The author responsible for distribution of materials integral to the findings presented in this article in accordance with the policy described in the Instructions for Authors ([www.plantphysiol.org](http://www.plantphysiol.org)) is: Yong-Eui Choi (yechoi@kangwon.ac.kr).

<sup>[W]</sup> The online version of this article contains Web-only data.

Article, publication date, and citation information can be found at [www.plantphysiol.org/cgi/doi/10.1104/pp.106.082743](http://www.plantphysiol.org/cgi/doi/10.1104/pp.106.082743).

species. Recently, we showed that the trichomes of tobacco exposed to  $\text{Cd}^{2+}$  and  $\text{Ca}^{2+}$  produced calcium (Ca)/cadmium (Cd)-containing grains (Choi et al., 2001, 2004; Choi and Harada, 2005). Other effects of Cd exposure were a retardation of plant growth and a 2-fold increase of the number of trichomes in comparison with untreated plants. Also, an increased concentration of Ca in the nutrient medium had a protective effect toward Cd toxicity and enhanced the production of the grains.

Trichomes are specialized unicellular or multicellular structures derived from the epidermal cell layer, which may have various functions depending on the plant species and organ (Rodriguez et al., 1983; Wagner et al., 2004). Tobacco has multicellular glandular trichomes of two types, the so-called long and short trichomes. The long trichomes are known to excrete various alkaloids, including nicotine, whereas the short ones excrete terpenoids (resins; Hallahan et al., 2000) and defensive proteins (Shepherd et al., 2005). The Ca/Cd-containing grains were 20 to 150  $\mu\text{m}$  in diameter and formed on head cells of both the short and long trichomes. They consisted in aggregates of micrometer-sized particles. Scanning electron microscopy coupled with energy dispersive x-ray fluorescence (SEM-EDX) analysis indicated the presence of minor amounts of magnesium (Mg), phosphorus (P), sulfur (S), and manganese (Mn), in addition to major amounts of Ca and Cd. Thus, these studies revealed a new function of tobacco trichomes: the excretion of Cd in the form of particles.

Other epidermal structures, the salt glands of *Armeria maritima* (Neumann et al., 1995), *Avicennia marina* (MacFarlane and Burchett, 1999), and *Silene vulgaris* (Bringezu et al., 1999), have been shown to excrete Ca/metal-containing grains. In contrast, nonglandular trichomes of several hyperaccumulating plants, including *Arabidopsis halleri* (Küpper et al., 2000; Zhao et al., 2000; Sarret et al., 2002) and *Alyssum* sp. (Broadhurst et al., 2004), and nonhyperaccumulating plants, including *Brassica juncea* (Salt et al., 1995), *Arabidopsis thaliana* (Ager et al., 2003; Domínguez-Solís et al., 2004), pumpkin (*Cucurbita moschata*; Iwasaki and Matsumura, 1999), and waterlily (*Nymphaea* sp.; Lavid et al., 2001), have been shown to sequester metals without apparent excretion. Trichomes of calcicolous plants also store large amounts of Ca. DeSilva et al. (1996) suggested that this could be a strategy to avoid the interference with stomatal functioning.

The mechanism of metal accumulation and excretion by trichomes and the binding environment of metals in these structures and their exudates are largely unknown. The aim of this work is to clarify several open questions that arose from our previous studies on tobacco and to extend it to zinc (Zn). The cation  $\text{Cd}^{2+}$  is frequently associated with  $\text{Ca}^{2+}$  in the environment because of their similar ionic radii. Does the production of Ca/metal grains occur for a cationic metal of different size from  $\text{Cd}^{2+}$ , such as  $\text{Zn}^{2+}$ ? If so, what is the influence of  $\text{Ca}^{2+}$  supply on the metal

uptake, translocation, and formation of the grains? Then, what is the mineralogical nature of the excreted Zn-containing grains, and what is the binding environment of Zn in the grains? This information is important because the chemical form of metals (inner or outer sphere complexes, coprecipitates with other metals, etc.) determines their mobility and their possible release in the environment. The most common biomineral formed by plants is  $\text{CaC}_2\text{O}_4$  mono- and dihydrate. However, various forms of  $\text{CaCO}_3$ , including amorphous  $\text{CaCO}_3$ , calcite, aragonite, and vaterite, are also synthesized by plants (Arnott and Pautard, 1970; Setoguchi et al., 1989). Another unknown is the mechanism of formation of the grains, which are generally larger than the trichome cells themselves. And, finally, what is the relative importance of metal excretion and accumulation in the leaf tissues?

To address these questions, tobacco plants were grown in hydroponics and in vitro in the presence of various concentrations of Ca and Zn. The effect of Ca on the short-term (24 h) and long-term (2 and 5 weeks) accumulation of Zn and on the production of the grains was studied. The endogenous accumulation of Zn in the top cells of trichomes was visualized under confocal laser scanning microscopy (CLSM) after labeling with Zinquin. The density of the trichomes was estimated by examining fresh leaves by variable pressure scanning electron microscopy (VP-SEM), and isolated grains were examined by variable pressure and standard scanning electron microscopy coupled with microanalysis (VP-SEM-EDX and SEM-EDX) and by a combination of three synchrotron-based techniques with a lateral resolution of a few micrometers. Specifically, the distribution of Ca and Zn in the grains was imaged by micro x-ray fluorescence ( $\mu\text{XRF}$ ), crystalline phases were identified by micro x-ray diffraction ( $\mu\text{XRD}$ ), and the binding environment of Zn was determined by Zn K-edge micro-extended x-ray absorption fine structure ( $\mu\text{EXAFS}$ ) spectroscopy.

## RESULTS

### Growth Retardation and Zn Accumulation in Tobacco Plants Treated with a Toxic Level of Zn in Hydroponic Culture

Seed-derived tobacco plants were grown on hydroponic culture containing a high level of Zn (0.25 mM) and with and without supplement of 3 mM of Ca (Table I; Fig. 1). The Zn toxicity was monitored by the growth of shoots and roots and by chlorophyll contents (Table II). After 2 and 5 weeks of toxic Zn treatment, both shoot and root growth were severely affected, and the chlorophyll content was markedly reduced. The growth inhibition was more severe for roots than for shoots, especially after 5 weeks of exposure. The supplementation with 3 mM Ca suppressed the growth inhibition effect but did not restore chlorophyll level. These results suggest that Ca alleviates some (but not all) of the toxic effects of Zn.

**Table I.** Culture conditions and investigations

Culture Conditions	Name of the Treatment	Total Ca Concentration in the Substrate	Total Zn Concentration in the Substrate	Duration of Exposure	Investigations	Grain Name
Hydroponic	Control	0.28 <sup>mM</sup>	$0.08 \times 10^{-3}$ <sup>mM</sup>	24 h, 2 and 5 weeks	Zn contents in shoots; root and shoot growth and chlorophyll content (2 and 5 weeks only); CLSM (2 weeks only)	
Hydroponic	Zn	0.28	0.25	24 h, 2 and 5 weeks	Zn contents in shoots; root and shoot growth and chlorophyll content (2 and 5 weeks only); CLSM (2 weeks only); SEM-EDX, $\mu$ XRD, $\mu$ XRF, and Zn $\mu$ EXAFS on isolated grains (5 weeks only)	Zn1, Zn2
Hydroponic	Zn + Ca	3.28	0.25	24 h, 2 and 5 weeks	Zn contents in shoots; root and shoot growth and chlorophyll content (2 and 5 weeks only); SEM-EDX, $\mu$ XRD, $\mu$ XRF, and Zn $\mu$ EXAFS on isolated grains (5 weeks only)	ZnCa1, ZnCa2, ZnCa3, ZnCa4
Hydroponic	Ca	3.28	$0.08 \times 10^{-3}$	5 weeks	SEM-EDX, $\mu$ XRD, and $\mu$ XRF on isolated grains	Ca1, Ca2
In vitro	In vitro-control	3	0.03	3 weeks	Shoot growth; size and number of grains; SEM-EDX on isolated grains; trichome density	
In vitro	In vitro-Zn	3	1	3 weeks	Shoot growth; size and number of grains; SEM-EDX on isolated grains; trichome density	
In vitro	In vitro-Zn + Ca	30	1	3 weeks	Shoot growth; size and number of grains; SEM-EDX on isolated grains; trichome density	

The analysis of total Zn content showed that the Ca supplement reduced the Zn accumulation in shoots after 24 h of Zn treatment (Table II). At the opposite, Zn accumulation was increased after 2 to 5 weeks of the same Zn + Ca treatment. Consequently, the protective effect of Ca cannot be explained by a competition between Ca and Zn resulting in a reduced Zn uptake.

#### Growth and Trichome Density and Grain Production in Tobacco Plants Cultured in Vitro

Growth retardation of tobacco plants cultured in vitro was similar to ex vitro culture in hydroponic medium. However, Zn accumulation of in vitro plants was lower (Tables II and III), although the in vitro growing medium contained higher Zn concentration than the hydroponic medium.

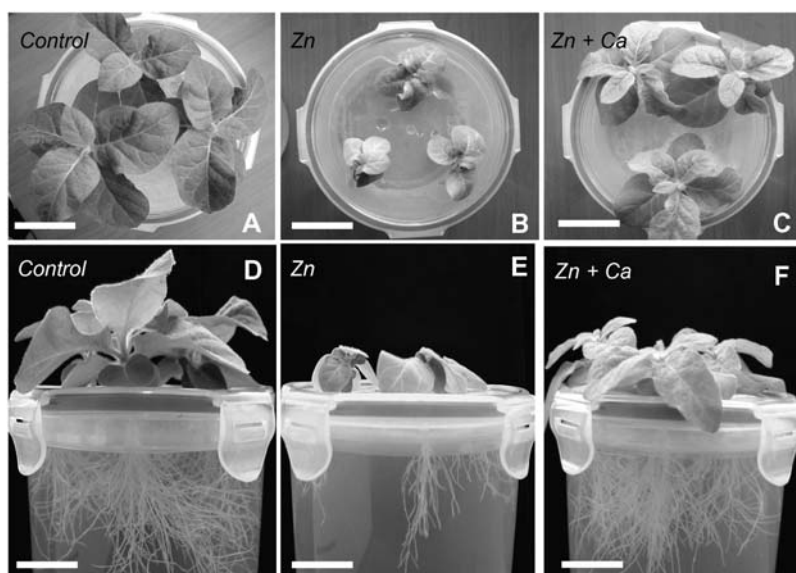


**Figure 1.** Tobacco plants grown for 2 weeks (A–C) and 5 weeks (D–F) in hydroponic medium containing  $0.08 \mu\text{M}$  Zn and  $0.28 \text{ mM}$  Ca (control),  $0.25 \text{ mM}$  Zn and  $0.28 \text{ mM}$  Ca (Zn), and  $0.25 \text{ mM}$  Zn and  $3.28 \text{ mM}$  Ca (Zn + Ca). Bars: A to C, 3.5 cm; D and E, 2.8 cm.

**Table II.** Plant growth, leaf chlorophyll contents, and Zn accumulation in shoots of tobacco grown under three conditions (culture conditions detailed in Table I)

Each value is the mean of three measurements on three different plants plus or minus the SD.

Treatment	Height of Shoot		Root Length		Chlorophyll Contents				Zn Accumulation in Shoot		
					2 Weeks		5 Weeks		24 h	2 Weeks	5 Weeks
	2 Weeks	5 Weeks	2 Weeks	5 Weeks	Chlorophyll a	Chlorophyll b	Chlorophyll a	Chlorophyll b			
	<i>cm</i>		<i>cm</i>		<i>mg g<sup>-1</sup> FW</i>				<i>μg g<sup>-1</sup> DW</i>		
Control	7.48 ± 0.46	11.3 ± 1.82	9.6 ± 1.6	20.4 ± 0.9	1.18 ± 0.211	0.34 ± 0.060	0.94 ± 0.049	0.29 ± 0.038	21.5 ± 3.5	36.2 ± 6.4	50.8 ± 9.3
Zn	2.46 ± 0.23	4.31 ± 0.37	6.2 ± 1.6	6.4 ± 1.0	0.67 ± 0.055	0.22 ± 0.031	0.26 ± 0.028	0.08 ± 0.008	326.4 ± 33.5	1,511.7 ± 31.6	2,309.0 ± 526.5
Zn + Ca	4.26 ± 0.37	6.37 ± 0.67	8.9 ± 1.0	10.0 ± 0.7	0.66 ± 0.103	0.21 ± 0.040	0.33 ± 0.063	0.10 ± 0.022	175.7 ± 28.2	2,783.9 ± 107.6	2,398.4 ± 182.4

This difference may result from a lower Zn bio-availability, respiration, and transpiration rates in vitro.

In vitro plants were used for counting the number of trichomes and isolating the grains because leaves of tobacco plants cultured ex vitro were more easily subjected to bacterial attack and contamination from aerosol particles. Leaves of the plants treated with or without Zn for 3 weeks were observed under VP-SEM (Table III; Fig. 2). There was no difference in trichome density for the mature leaves. At the opposite, the young leaves of plants exposed to Zn and Zn + Ca showed a more than 2-fold increase of the density of long and short trichome relative to the control (Fig. 2, A–C). No difference of leaf size was observed between the various treatments, so this increase was real. This suggests a possible role of Zn in the trichome development. Figure 2B showed that the length and the volume of the trichomes were increased upon Zn treatment, although epidermal cells and stomatal opening looked smaller than those of control. A number of grains were observed on the top of both short and long trichomes, as seen in Figure 2C (arrows). For each treatment, the grains were collected and observed by VP-SEM (Table III; Fig. 2, D–F). Their number and their mean size increased in the following order: in vitro-Zn-Ca treatment > in vitro-Zn > in vitro-control (Table III; Fig. 2, D–F). We showed previously that exposure to 30 mM Ca without Zn (Ca treatment) did not enhance the production of the grains but stimulated the formation of intracellular Ca-containing crystals in leaves (Choi and Harada, 2005).

The same general trends in trichome density and grain production were observed on plants grown hydroponically. The amount of Zn excreted per plant was estimated based on the number and size of grains per shoot and their Zn content calculated using the ZAF (atomic number, absorption, fluorescence correction) method (Goldstein et al., 1981). We found 4.1 and 11.0 μg of Zn per plant under the in vitro-Zn and in vitro-Zn + Ca treatment, respectively, which corresponds to 9.2% and 16.9% of total Zn in the leaves, respectively. Note that these values reflect the grains present on the leaves after 3 weeks of exposure, not the total amount of Zn excreted during the experiment.

#### Confocal Imaging of Zn Accumulation in Trichome Cells after Zinquin Labeling

Tobacco plants were grown hydroponically with 0.25 mM Zn + 0.28 mM Ca (Zn treatment) and 0.08 μM Zn + 0.28 mM Ca (control) for 2 weeks. Zn distribution on the leaf surfaces was investigated by CLSM after treatment with Zinquin (Fig. 3). Zinquin ethyl ester is a lipo-soluble fluorescence dye that has been used to detect intracellular Zn ions in animal cells (Coyle et al., 1994). This study shows that it can be used on plant cells too. For control plants, a faint fluorescence was detected in the trichomes (Fig. 3, A and C). For Zn-treated plants, Zn was preferentially accumulated in head cells of both short and long trichomes (Fig. 3, B and D). Extracellular crystals were not present on the top of the trichomes observed by CLSM because they

**Table III.** Shoot growth parameters and Zn content, number of trichomes, and grain production by the leaves of tobacco plants cultured in vitro for 3 weeks under three conditions (culture conditions given in Table I)

Each value is the mean of three individual measurements plus or minus SD. The number of trichomes and grain production were determined by VP-SEM observations.

Treatment	Height of Shoot	Shoot Dry Weight	Zn Accumulation in Shoot	No. of Trichomes per cm <sup>2</sup> of Leaf		Grain Production and Zn Excretion per Plant			
				Short Trichome	Long Trichome	No. of Grains	Size of Grains	Excreted Zn <sup>a</sup>	Excreted Zn <sup>b</sup>
	<i>cm</i>	<i>mg</i>	<i>μg g<sup>-1</sup> DW</i>				<i>μm</i>	<i>μg</i>	<i>%</i>
In vitro-control	8.7 ± 0.56	171 ± 12.3	91.7 ± 12.2	21 ± 3.7	14 ± 2.3	127 ± 34	26 ± 11.2	–	–
In vitro-Zn	4.4 ± 0.33	80 ± 6.5	564.0 ± 36.2	56 ± 7.3	38 ± 4.2	784 ± 216	57 ± 12.8	4.1	9.2
In vitro-Zn + Ca	6.4 ± 0.45	97 ± 9.3	675.0 ± 33.5	43 ± 5.7	25 ± 6.3	1,223 ± 245	86 ± 13.2	11.0	16.9

<sup>a</sup>Excreted Zn was calculated based on the number and size of excreted grains (Zn content was 2% in Zn grain, 1% in Zn + Ca grain, as estimated by ZAF method). <sup>b</sup>Percentage of excreted Zn was calculated based on Zn amount in shoot.

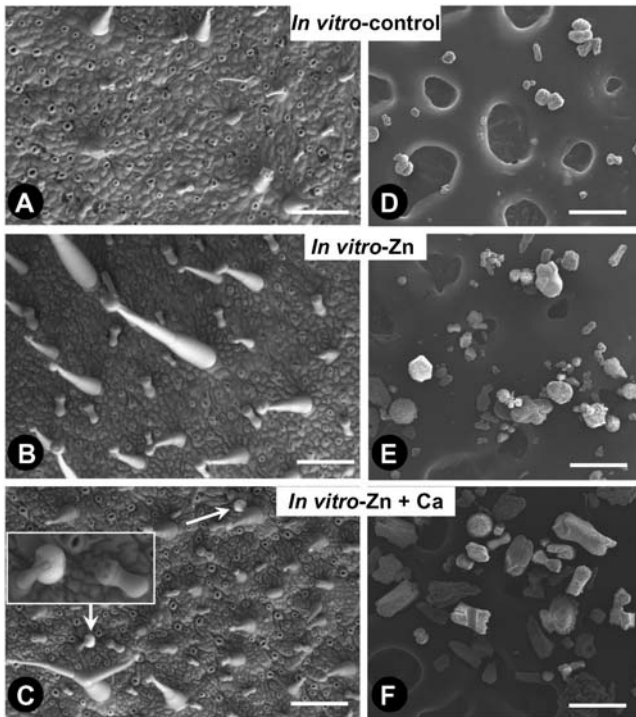


**Figure 2.** VP-SEM observation of the third leaf from the top (A–C) and of isolated grains (D–F) of tobacco grown *in vitro* for 3 weeks in a medium containing 0.03 mM Zn and 3 mM Ca (control), 1 mM Zn and 3 mM Ca (Zn), and 1 mM Zn and 30 mM Ca (Zn + Ca). Bars: A to C, 150  $\mu\text{m}$ ; D and E, 200  $\mu\text{m}$ .

fell off during the Zinquin treatment. Fluorescence was also detected in the epidermal surfaces of the leaves but was always less dense than in the trichome cells (data not shown).

#### Zn Distribution Analysis by $\mu\text{XRF}$ Spectrum

The distribution of Ca and Zn in the leaves of tobacco exposed to 0.25 mM Zn + 3.28 mM Ca (Zn + Ca treatment) was imaged by synchrotron-based  $\mu\text{XRF}$  (Fig. 4). Zn was systematically more concentrated in veins and trichomes, with the short trichomes being about 5 times richer than the long trichomes. Short trichomes were also rich in Ca but in the same proportion as Zn (i.e. the Ca  $K_{\alpha}$ :Zn  $K_{\alpha}$  ratio equaled about 1 in the two types of trichomes). No grains were observed at the top of the trichomes because they fell off during the sample preparation, such as freeze-drying and mounting and its rastering under the x-ray beam, but some were still detected as Zn hot-spots on the leaf surfaces.

#### Morphology, Chemical Composition, and Solubility of the Grains

Some grains present on the surface of a fresh leaf from a Zn-treated plant were studied by VP-SEM-EDX (Fig. 5A), and other grains produced under various

conditions (*in vitro* and hydroponic culture with various Ca and Zn concentrations; Table I) were collected and studied by VP-SEM-EDX and SEM-EDX (Fig. 5, B–H). The size of the grains varied from 10  $\mu\text{m}$  to 150  $\mu\text{m}$  in diameter for all treatments. A variety of globular to crystal-like shapes were observed. In most cases, grains consisted in aggregates of small (<1  $\mu\text{m}$ ) particles, as previously observed for  $\text{Cd}^{2+}$ -treated plants (Choi et al., 2001, 2004). The globular grains generally were made of concentric layers (e.g. Fig. 5E). No particular relationship could be established between the grain morphology and the type of treatment.

Ca was always the major element, even for plants grown on 0.28 mM Ca. In contrast, Zn was not detected in the grains when its concentration in the nutrient solution was low (Ca treatment, 0.08  $\mu\text{M}$  Zn + 3.28 mM Ca). In grains from the Zn + Ca-treated plants (0.25 mM Zn + 3.28 mM Ca), the Zn  $K_{\alpha}$  fluorescence peak was small (Zn concentration ranged from 1–5 weight [wt] %), as estimated by the ZAF method, and it was occasionally more intense (Zn concentration ranged from 2–40 wt %) in grains from the Zn-treated plants (0.28 mM Ca + 0.25 mM Zn). Minor elements included oxygen (O), Mg, silicon (Si), P, S, chlorine (Cl), potassium (K), and Mn (carbon [C] could not be measured because the grains were coated with C). No particular relationship could be established between the concentration of the minor elements and the type of treatment, except for Mn that was not detected in grains from the Zn + Ca

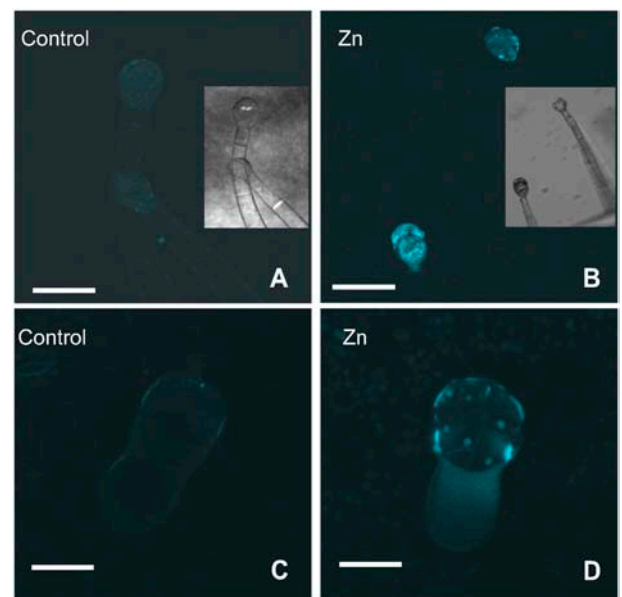


**Figure 3.** Distribution of Zn in long (A and B) and short (C and D) trichomes of tobacco obtained by confocal microscopy using Zinquin fluorescent dye. Insets in A and B show optical microscope images. Plants were grown in hydropony in control (0.08  $\mu\text{M}$  Zn and 0.28 mM Ca) and Zn treatment (0.25 mM Zn and 0.28 mM Ca) for 2 weeks. The Zn signal is faint and almost evenly distributed in the trichomes of control plants, whereas the trichomes of Zn-treated plants (particularly the long ones) show a high concentration of Zn in the head cells. Bars: A and B, 70  $\mu\text{m}$ ; C and D, 86  $\mu\text{m}$ .

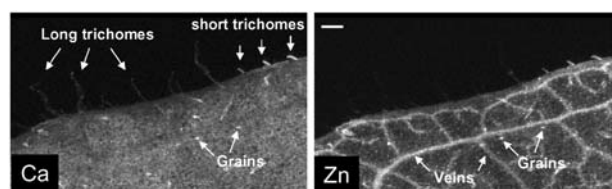


**Figure 4.** Distribution of Ca and Zn determined by  $\mu$ XRF in a freeze-dried leaf of tobacco exposed to 0.25 mM ZnSO<sub>4</sub> + 3.28 mM CaCl<sub>2</sub> for 5 weeks (Zn + Ca treatment). The long trichomes are rich in Ca, whereas the short trichomes are rich in Ca and Zn. The veins are richer in Zn than the leaf tissues. Bar = 300  $\mu$ m.

treatment. There was no morphological or compositional difference between grains observed directly on the leaves using VP-SEM and grains isolated by water extraction or using toothpicks. The solubility of the grains in water was tested in a wide range of pH. They were insoluble between pH 4 and 12.5 and soluble in acidic conditions; they were dissolved within 10 min at pH 3 and within 2 min at pH 2. Therefore, the structure and the composition of the grains are supposed to be preserved during the water extraction.

#### $\mu$ XRD Analysis of the Grains

The grains produced by tobacco plants grown in hydroponics under the three treatments (Ca, Zn, and Zn + Ca) were also analyzed by  $\mu$ XRD (Fig. 6). Five to 10 grains per type of treatment were examined. For each grain,  $\mu$ XRD patterns from a  $16 \times 7 \mu\text{m}^2$  spot of the Ca-richest region (Ca treatment) or the Zn-richest region (Zn and Zn + Ca treatment) and of the whole grain were recorded. The point and average patterns were the same, except that the Debye rings for the second were less intense and longer (i.e. more powder like). Therefore, either the Ca- and Zn-richest regions are representative of the structural composition of the entire grains, or the other regions contain amorphous material. Figure 6, A and B, shows the two-dimensional  $\mu$ XRD patterns for two grains produced under the Ca treatment (grains Ca1 and Ca2). The diameter of these grains is about 50  $\mu\text{m}$ . Bragg reflections for grain Ca1 consist of portions of Debye rings, indicating that the grain is composed of submicrometric crystals (Manceau et al., 2002). The intensities along each ring (constant Bragg angle) were integrated to obtain the one-dimensional XRD pattern presented in Figure 6C. The XRD peaks are slightly shifted to higher angles (i.e. smaller  $d$  values) relative to those of calcite (CaCO<sub>3</sub>), indicating smaller unit cell parameters. The refined parameters were  $a = 4.929 \text{ \AA}$  and  $c = 16.754 \text{ \AA}$ , compared to  $a = 4.9896$  and  $c = 17.0610 \text{ \AA}$  for pure calcite (Supplemental Table I). The contraction of the unit cell is likely due to the substitution of smaller cations for Ca. Based on  $\mu$ XRF analyses, Mn is a possible substituent for Ca. This particular grain was not analyzed by SEM-EDX, so the presence of light elements ( $Z < 20$ ) could not be tested. However, Mg

was frequently detected by SEM-EDX in other grains from the same treatment (Fig. 5F; data not shown). As divalent Mn (0.67  $\text{\AA}$ ) and Mg (0.72  $\text{\AA}$ ) have a smaller ionic radius than Ca<sup>2+</sup> (1.00  $\text{\AA}$ ; Shannon, 1976), these two impurities are good candidate species for substitution at the Ca site. Assuming the presence of only one substitutional atom, the stoichiometry of the Ca1 grain was calculated from the experimental  $a$  and  $c$  unit cell parameters using the Vegard law (West, 1984). Briefly, this approach allows the determination of the composition of a binary solid solution from the linear regression between the composition and the unit cell parameters of the two pure end-members. Two independent calculations were performed with either  $a$  or  $c$ . The difference in the stoichiometry coefficients obtained by the two calculations was below 0.02 atom for all grains. For the Mg substitution, the end-members were calcite and magnesite (MgCO<sub>3</sub>), and the calculated formula for grain Ca1 was Ca<sub>0.84</sub>Mg<sub>0.16</sub>CO<sub>3</sub>. For the Mn substitution, the end-members were calcite and rhodocrosite (MnCO<sub>3</sub>), and the calculated formula was Ca<sub>0.75</sub>Mn<sub>0.25</sub>CO<sub>3</sub>. As the two impurities may be present in the grain, the proposed formula is Ca<sub>(0.84 - 0.09X)</sub>Mg<sub>[0.16(1 - X)]</sub>Mn<sub>(0.25X)</sub>CO<sub>3</sub>, with X varying from 0 to 1. Whewellite (CaC<sub>2</sub>O<sub>4</sub> · H<sub>2</sub>O) was also detected in grain Ca1. This mineral has several XRD peaks at the same position as those from the substituted calcite crystallites, but the peak at  $Q = 1.058 \text{ \AA}^{-1}$  ( $d = 5.94 \text{ \AA}$ ) is characteristic of this species, thereby allowing its unambiguous identification (Fig. 6C). This peak appears as a spotty feature on the two-dimensional pattern (labeled W in Fig. 6A), which indicates that whewellite is coarsely crystalline at the scale of the x-ray probe ( $16 \times 7 \mu\text{m}^2$ ). One XRD reflection was attributed to vaterite. This latter mineral was more definitely identified in another experiment, in which tobacco was exposed to Cd<sup>2+</sup> (data not shown).

The  $\mu$ XRD pattern for grain Ca2 is spotty (Fig. 6B), which is indicative of coarse crystals. Most of x-ray reflections correspond to substituted calcite and have an intermediate position between those of pure calcite and grain Ca1 (inset in Fig. 6C for the Bragg reflection 113), which suggests a lower degree of substitution relative to grain Ca1. The average structural formula of this grain was calculated following the same procedure as for grain Ca1, but, because of the smaller number of diffraction peaks, only the  $a$  parameter was refined (Supplemental Table I). Calculation yielded Ca<sub>(0.91 - 0.05X)</sub>Mg<sub>[0.09(1 - X)]</sub>Mn<sub>(0.14X)</sub>CO<sub>3</sub>, with X varying from 0 to 1. Fewer peaks, attributed to whewellite, weddellite (CaC<sub>2</sub>O<sub>4</sub> · 2 H<sub>2</sub>O), and vaterite (CaCO<sub>3</sub>), also were detected (Fig. 6C).

Figure 7 shows  $\mu$ XRD data for two grains produced under the Zn + Ca treatment (0.25 mM Zn + 3.28 mM Ca). These grains were rich in Ca and Zn, with the two elements being heterogeneously distributed within the grains (average Zn:Ca K $\alpha$  ratio = 7.5 and 1 for grains ZnCa1 and ZnCa2, respectively). The  $\mu$ XRD pattern for grain ZnCa1 exhibits discontinuous rings as well as

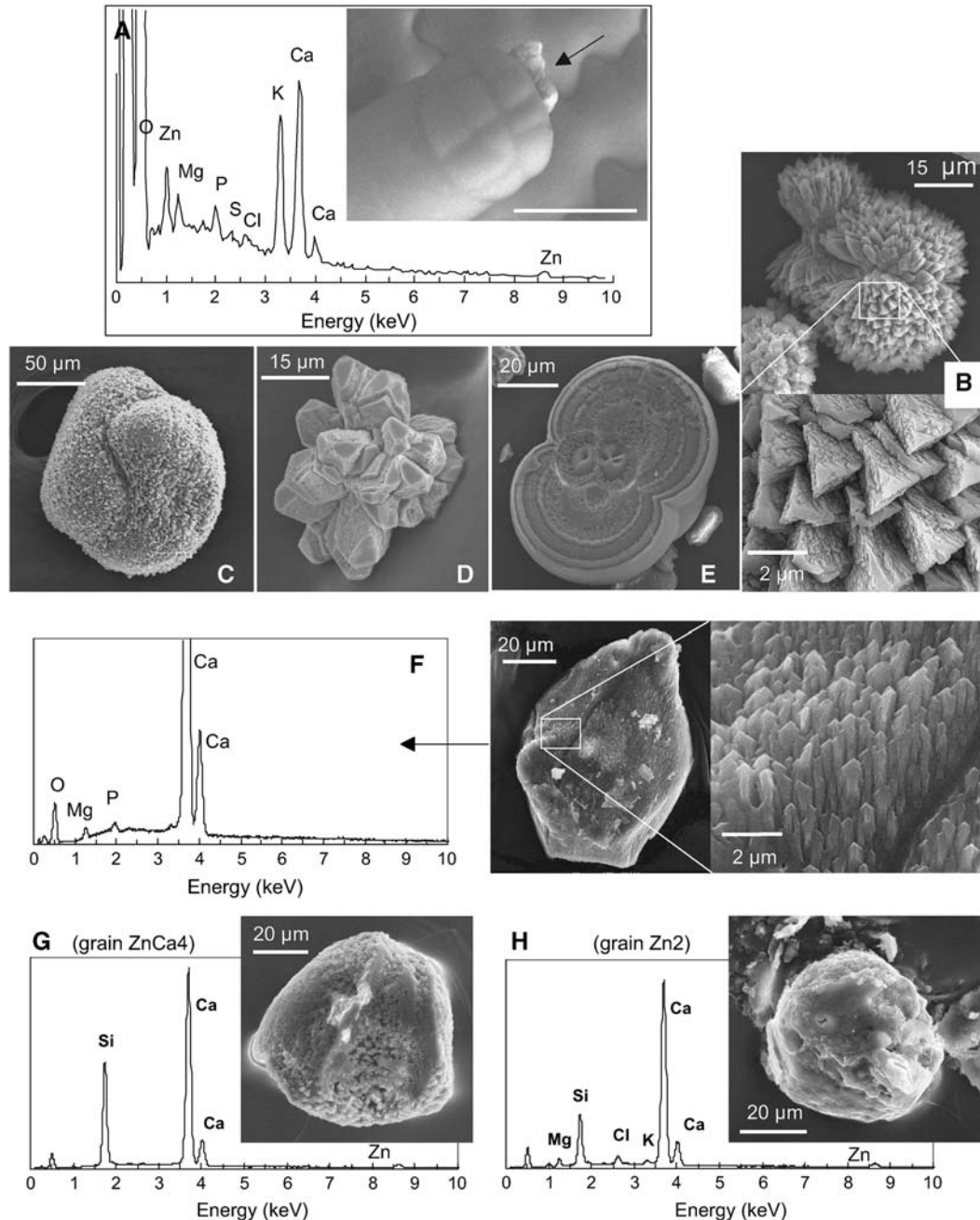


**Figure 5.** A, Representative VP-SEM image and EDX spectrum of a grain present at the top of a trichome of tobacco plant grown in hydroponic culture under Zn treatment. B to H, VP-SEM (B–E) and SEM (F–H) images and EDX spectra of grains produced by tobacco plants grown in vitro (B–E) and hydroponically (F–H) under the various conditions listed in Table I. B and C, In vitro-control; D, in vitro-Zn; E, in vitro-Zn + Ca; F, Ca; G, Zn + Ca; H, Zn. EDX spectra were recorded at 20 kV.

isolated spots (Fig. 7C). As for grains Ca1 and Ca2, the incomplete rings correspond to substituted calcite. Zn is a likely substitute atom but not Mn because it was not detected in this grain (Fig. 7B). The presence of Mg was not tested by SEM-EDX but is possible. The chemical formula of this grain calculated with smithsonite ( $\text{ZnCO}_3$ ) as Zn end-member and magnesite as Mg end-member is  $\text{Ca}_{0.84}(\text{Mg,Zn})_{0.16}\text{CO}_3$  (Supplemental Table I).  $\text{Mg}^{2+}$  and  $\text{Zn}^{2+}$  have similar ionic

radii (0.72 and 0.75 Å; Shannon, 1976) and, consequently, undergo similar reduction of the crystal lattice parameters. The isolated spots were attributed to whewellite. The  $\mu\text{XRD}$  pattern for grain ZnCa2 exhibited also incomplete Debye rings (data not shown). All peaks were attributed to  $\text{Ca}_{0.92}(\text{Mg,Zn})_{0.08}\text{CO}_3$  crystals. The lower degree of substitution of calcite in grain ZnCa2 compared to grain ZnCa1 is reflected in the  $\mu\text{XRD}$  pattern by a smaller shift of its peaks relative to

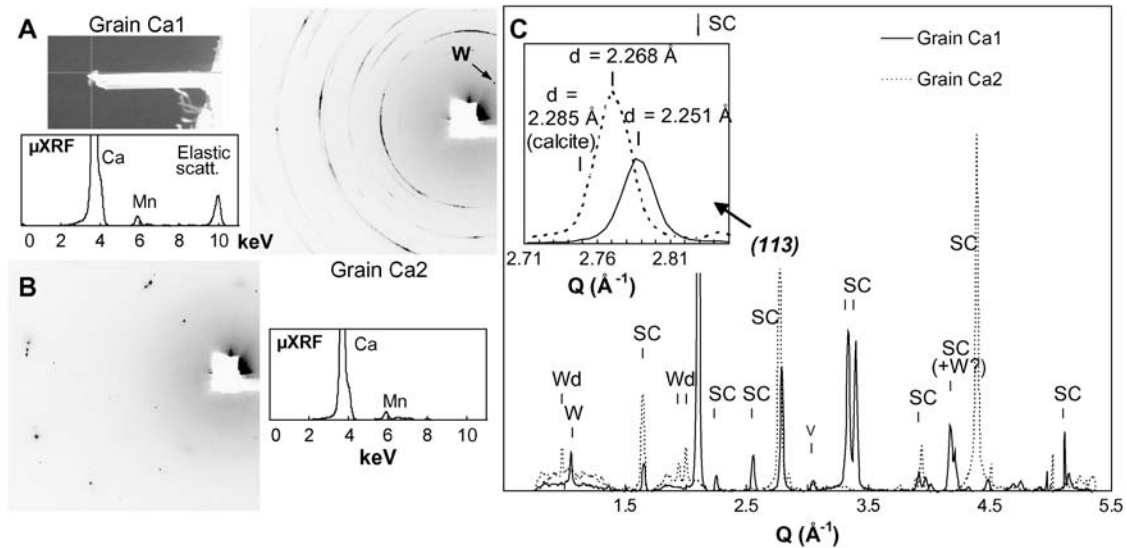


**Figure 6.** A and B,  $\mu$ XRD patterns and  $\mu$ XRF spectra for grains Ca1 (A) and Ca2 (B) produced by the trichomes of a tobacco plant exposed to 3.28 mM Ca for 5 weeks (Ca treatment). The picture in A shows the grain mounted at the tip of a glass capillary. C, One-dimensional XRD patterns of the two grains. Grain Ca1 contains polycrystalline substituted calcite particles (SC) of estimated composition  $\text{Ca}_{(0.84 - 0.09X)}\text{Mg}_{(0.16(1 - X))}\text{Mn}_{(0.25X)}\text{CO}_3$ , with X varying from 0 to 1, and coarse whewellite crystals (W,  $\text{CaC}_2\text{O}_4 \cdot \text{H}_2\text{O}$ ). Grain Ca2 contains polycrystalline calcite particles (SC) of estimated composition  $\text{Ca}_{(0.91 - 0.05X)}\text{Mg}_{(0.09(1 - X))}\text{Mn}_{(0.14X)}\text{CO}_3$ , with X varying from 0 to 1, and whewellite (W,  $\text{CaC}_2\text{O}_4 \cdot \text{H}_2\text{O}$ ), weddellite (Wd,  $\text{CaC}_2\text{O}_4$ ), and vaterite (V,  $\text{CaCO}_3$ ) coarse crystals. The shift to lower  $d$  values (higher  $Q$  values) of the diffraction peaks for grain Ca1 relative to grain Ca2 indicates that the former contains more impurities (i.e. higher substitution degree). Inset, Enlargement of the 113 reflections of the two grains. The peak position of pure calcite is indicated by a vertical bar.

calcite (inset in Fig. 7D for the Bragg reflections 110 and 113).

Another form of  $\text{CaCO}_3$ , aragonite, was identified in grain ZnCa3 from the Zn + Ca treatment (Fig. 8).

This grain also contained Zn-substituted calcite ( $\text{Ca}_{0.93}\text{Zn}_{0.07}\text{CO}_3$ ). The continuous Debye rings observed in Figure 8A correspond to aragonite, and the incomplete rings and speckles correspond to

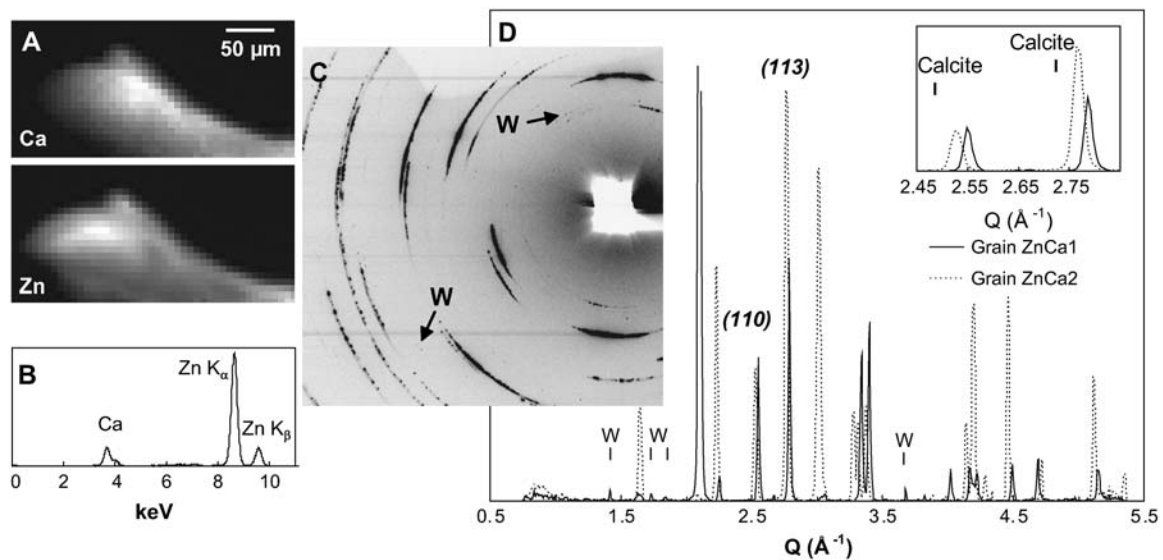


**Figure 7.** A, Ca and Zn distributions for grain ZnCa1 produced by tobacco exposed to 0.25 mM Zn + 3.28 mM Ca for 5 weeks. B,  $\mu$ XRF spectrum of the same grain recorded at an incident energy of 17 keV on the Zn-richest spot. C,  $\mu$ XRD pattern of the whole grain. D, One-dimensional XRD patterns for grains ZnCa1 and ZnCa2 produced in the same conditions. Grain ZnCa1 contains substituted calcite [unlabeled peaks,  $\text{Ca}_{0.84}(\text{Mg,Zn})_{0.16}\text{CO}_3$ ] and whewellite (W,  $\text{CaC}_2\text{O}_4 \cdot \text{H}_2\text{O}$ ), and ZnCa2 contains substituted calcite [all peaks,  $\text{Ca}_{0.92}(\text{Mg,Zn})_{0.08}\text{CO}_3$ ] only. Similar to grains Ca1 and Ca2, the higher the degree of substitution, the larger is the shift of the XRD peaks toward the low  $d$  values (or high  $Q$  values) relative to pure calcite (inset).

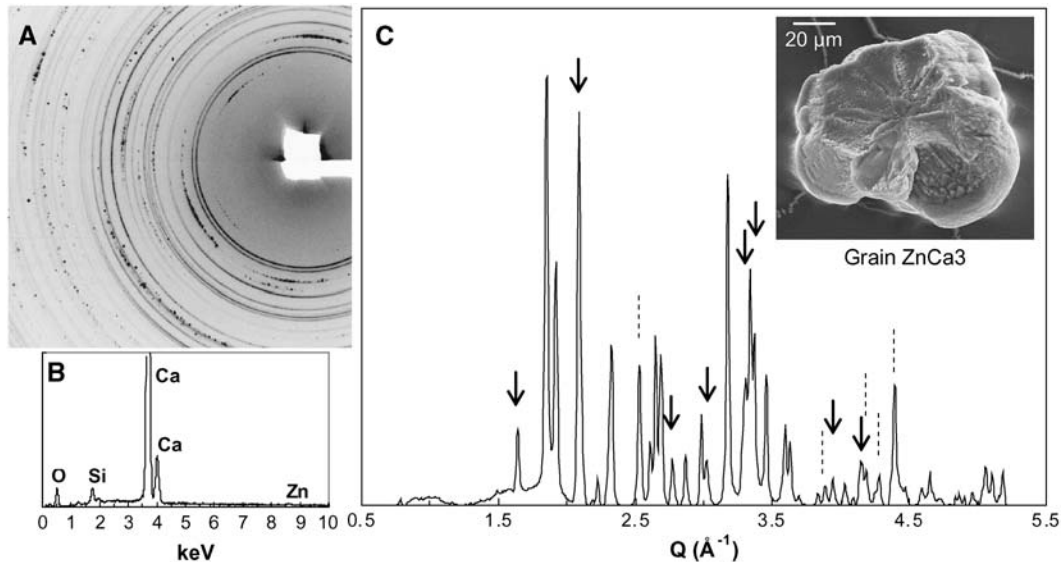


**Figure 8.** A, Two-dimensional XRD pattern for grain ZnCa3 produced by tobacco exposed to 0.25 mM Zn + 3.28 mM Ca for 5 weeks. B, EDX spectrum recorded at 20 kV. C, One-dimensional XRD pattern. Arrowed peaks correspond to substituted calcite [ $\text{Ca}_{0.93}(\text{Mg,Zn})_{0.07}\text{CO}_3$ ], peaks noted by a dashed line correspond to substituted calcite and aragonite, and all other peaks correspond to aragonite. Inset, SEM image of the grain.

substituted calcite. Thus, aragonite occurs as nanoparticles, whereas substituted calcite occurs as submicrometric crystals. Another grain (ZnCa4) contained  $\text{Ca}_{0.87}\text{Zn}_{0.13}\text{CO}_3$  (Supplemental Table I; Supplemental Fig. 1). For ZnCa3 and ZnCa4, Zn was the only substitute atom because neither Mg nor Mn was detected by  $\mu\text{XRF}$  and SEM-EDX (Figs. 8B and 5G for the EDX spectra;  $\mu\text{XRF}$  spectra not shown).

Several grains produced under the Zn treatment contained (Mg,Zn)-substituted calcite (e.g. grain Zn1; Supplemental Table I; Supplemental Fig. 2), and other grains (e.g. grain Zn2; Fig. 5H) did not produce *hkl* reflections, although they also contained Zn and Ca. The amorphous nature of these grains was confirmed by Zn-EXAFS (see below) and by Ca-x-ray absorption near-edge structure spectroscopy (data not shown).

In conclusion, submicrometer-sized calcite crystals substituted by Zn, Mg, and Mn were the most frequent mineral species. Other minerals identified include, by decreasing order of abundance, whewellite (always coarsely crystalline), weddellite, aragonite, and vaterite.  $\text{ZnC}_2\text{O}_4$  was never detected. Zn-containing grains were also analyzed by Zn K-edge  $\mu\text{EXAFS}$  spectroscopy to confirm the presence of Zn-substituted calcite, to gain more insight on the nature of the amorphous or poorly crystallized Zn species, and to determine the proportions of all Zn phases in case of mixture.

#### Zn K-Edge $\mu\text{EXAFS}$ Analysis of the Grains

Figure 9 shows the Zn  $\mu\text{EXAFS}$  spectra of the Zn-richest regions for the grains. Spectra with several frequencies (e.g. ZnCa1 and ZnCa2) are indicative of a long-range ordered Zn-binding environment, such as

that in a mineral structure, whereas spectra dominated by a single frequency (e.g. Zn2) are indicative of a short-range ordered Zn environment. Spectra ZnCa3, ZnCa4, and Zn1 are somehow intermediate between the two previous sets of spectra, suggesting a mixture of Zn species. Data analysis was done by linear combination fits using an extended database of Zn reference compounds containing Zn-bearing and Zn-sorbed minerals, Zn precipitates, and Zn complexed to simple organic acids and complex biopolymers (Sarret et al., 2004; Guiné et al., 2006). One- to three-component simulations were tested. All spectra were reproduced correctly with two components (Fig. 9; Table IV). Adding a third one did not improve the fit quality significantly, as indicated by the normalized sum-squares residual parameter (*NSS*) because its value decreased by less than 10% upon adding a third component.

Spectra ZnCa1 and ZnCa2 show a marked similarity to that of Zn-substituted calcite, the major difference being a smaller amplitude of the unknowns. Accordingly, the best one-component fits for these two samples were obtained with Zn-substituted calcite (Table IV; dashed lines for ZnCa1 in Fig. 9). The wave frequencies and overall shapes of the unknowns were satisfactorily reproduced by this model compound but not the amplitude at low *k*. Adding a second component greatly improved the simulations. Fits of equivalent quality were obtained with either Zn-humic acid complex (Zn-organic acids in Table IV) or Zn-sorbed hydroxylapatite (Zn-sorbed phosphate) as second component. Zn complexes with simple organic acids (oxalate, citrate, malate, etc.) were tested also but did not provide satisfactory fits. The

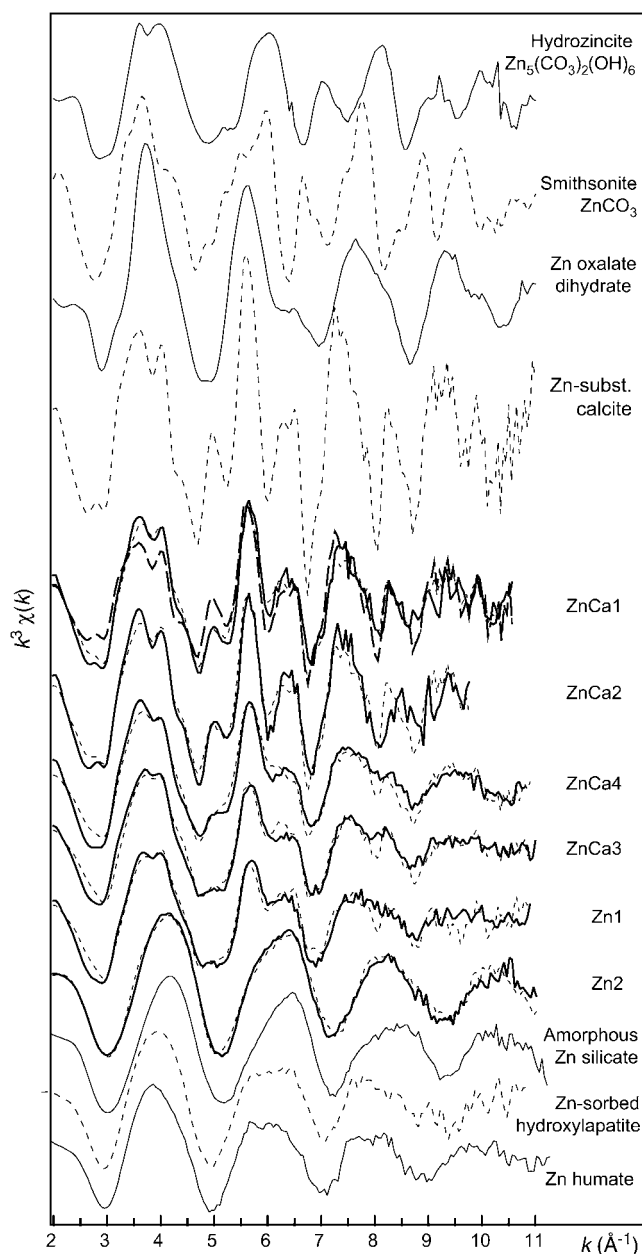


**Figure 9.** Zn bulk EXAFS spectra for selected Zn reference compounds, and Zn  $\mu$ EXAFS spectra for grains produced by tobacco exposed for 5 weeks to 0.25 mM Zn + 3.28 mM Ca (ZnCa1, ZnCa2, ZnCa3, and ZnCa4) and to 0.25 mM Zn (Zn1 and Zn2). Solid line, Experimental data; dashed line, one-component fit (for ZnCa1 only); dotted line, two-component fit.

Zn-humic acid complex reference was used as a proxy for Zn bonded to multiple functional groups, including carboxyl, hydroxyl, and phenol groups. This component species may correspond to organic compounds excreted by the trichomes. Crystalline Zn phosphate compounds, including Zn phosphate tetrahydrate (hopeite and parahopeite) and Zn phosphate dihydrate, did not provide good fits to the data. For technical reasons, grains ZnCa1 and ZnCa2 were not

analyzed by SEM-EDX; consequently, the presence of P could not be verified by chemical analysis. However, this element was frequently detected in grains from the three treatments, as shown for the Ca treatment in Figure 5F. Therefore, Zn-organics and Zn phosphate forms are equally probable species in grains ZnCa1 and ZnCa2. The presence of Zn in calcite is consistent with  $\mu$ XRD results for the two grains. Note that calcite grains may also contain Mg since this element was often detected by SEM-EDX.

Spectra ZnCa3, ZnCa4, and Zn1 were simulated correctly by a mixture of Zn-substituted calcite and Zn-organic acids ( $NSS = 7.2, 7.9,$  and  $4.8,$  respectively; Table IV). The fractional amount of Zn-substituted calcite (15%–23%) is lower than that in grains ZnCa1 and ZnCa2 (40%–53%), in agreement with the spectral differences of the two sets of grains (see above). Simulations with Zn-sorbed phosphate instead of Zn-organic acids were much weaker ( $NSS = 0.136, 0.120,$  and  $0.098,$  respectively). This result is consistent with the absence of P in ZnCa4 and Zn1 (Fig. 5G; Supplemental Fig. 2B), and its trace amounts in ZnCa3 (Fig. 8B). Again, the occurrence of Zn-substituted calcite in grains ZnCa3, ZnCa4, and Zn1 is consistent with  $\mu$ XRD results.

The incorporation of Zn in the aragonite crystallites from grain ZnCa3 was not tested because of the lack of Zn-substituted aragonite reference. However, this species is unlikely, or at most minor, for two reasons. First,  $\mu$ XRD data showed that this carbonate species is not substituted, in contrast to calcite. Second, the EXAFS spectrum of Zn-substituted aragonite would be different from that of Zn-substituted calcite because these two carbonate polymorphs do not have the same structure. The fact that the sum of the contributions from individual reference spectra to all sample spectra (except ZnCa4) is  $100\% \pm 10\%$  adds further credibility to the determined speciation. The lower sum for ZnCa4 (i.e. 80%) probably results from an overabsorption effect (Manceau et al., 2002). This effect decreases the amplitude of the measured signal without modifying the relative contributions of the component spectra.

Spectrum Zn2 was reproduced best with a combination of Zn-sorbed silica and Zn-organic acids. The presence of Si was confirmed by SEM-EDX (Fig. 5H). Zn-sorbed phosphate also provided a good fit to the data ( $NSS = 2.9$ ), but this model was rejected because the grain did not contain P. The absence of Zn-substituted calcite in this grain is consistent with the lack of diffraction peaks on the  $\mu$ XRD pattern.

In conclusion, the EXAFS analysis engenders confidence in the presence of Zn-substituted calcite thanks to the unique spectral signature of this species and to the consistency in the interpretations of the spectroscopic and diffraction data. In addition, this species is logically more abundant in the Zn + Ca treatment than in the Zn treatment. EXAFS spectroscopy is less sensitive to Zn-sorbed silica, Zn-sorbed phosphate, and Zn-organic acids as a result of the short-range order of

**Table IV.**  $\mu$ EXAFS and  $\mu$ XRD results

Grain	Proportion of Zn Species (%) Determined by Linear Combination Fitting the $\mu$ EXAFS Spectra				Sum	NSS <sup>b</sup>	Elements Detected by SEM-EDX and/or $\mu$ XRF <sup>a</sup>	Minerals Identified by $\mu$ XRD
	Zn-Substituted Calcite	Zn-Organic Acids	Zn-Sorbed Silica	Zn-Sorbed Phosphate				
%								
Grains from the Ca treatment <sup>c</sup>								
Ca1							Ca, Mn (elements lighter than Ca not analyzed)	Subst. calcite (Ca <sub>(0.84 - 0.09X)</sub> Mg <sub>[0.16(1 - X)]</sub> Mn <sub>(0.25X)</sub> CO <sub>3</sub> ), whewellite (CaC <sub>2</sub> O <sub>4</sub> , H <sub>2</sub> O)
Ca2							Ca, Mn (elements lighter than Ca not analyzed)	Subst. calcite (Ca <sub>(0.91 - 0.05X)</sub> Mg <sub>[0.09(1 - X)]</sub> Mn <sub>(0.14X)</sub> CO <sub>3</sub> ), whewellite (CaC <sub>2</sub> O <sub>4</sub> , H <sub>2</sub> O), weddellite (CaC <sub>2</sub> O <sub>4</sub> , 2 H <sub>2</sub> O), vaterite (CaCO <sub>3</sub> )
Grains from the Ca + Zn treatment <sup>c</sup>								
ZnCa1	53	–	–		53	23.6 <sup>d</sup>	Zn, Ca (elements lighter than Ca not analyzed)	Subst. calcite (Ca <sub>0.84</sub> (Mg,Zn) <sub>0.16</sub> CO <sub>3</sub> ), whewellite (CaC <sub>2</sub> O <sub>4</sub> , H <sub>2</sub> O)
	40	50	–	–	90	8.9 <sup>d</sup>		
	44	–	–	49	93	9.5		
ZnCa2	59	–	–	–	59	18.9	Zn, Ca (elements lighter than Ca not analyzed)	Subst. calcite (Ca <sub>0.92</sub> (Mg,Zn) <sub>0.08</sub> CO <sub>3</sub> )
	50	39	–	–	89	11.3 <sup>d</sup>		
	53	–	–	38	91	11.7		
ZnCa3	22	78	–	–	100	7.2 <sup>d</sup>	Zn, Ca, Si, O	Subst. calcite (Ca <sub>0.93</sub> Zn <sub>0.07</sub> CO <sub>3</sub> ), aragonite (CaCO <sub>3</sub> )
ZnCa4	23	57	–	–	80	7.9 <sup>d</sup>	Zn, Ca, Si, O	Subst. calcite (Ca <sub>0.87</sub> Zn <sub>0.13</sub> CO <sub>3</sub> )
Grains from the Zn treatment <sup>c</sup>								
Zn1	15	73	–	–	88	4.8 <sup>d</sup>	Zn, Ca, K, Cl, Si, Mg, O	Subst. calcite (Ca <sub>0.92</sub> (Mg,Zn) <sub>0.08</sub> CO <sub>3</sub> )
Zn2	–	37	79	–	115	2.7 <sup>d</sup>	Zn, Ca, K, Cl, Si, Mg, O	

<sup>a</sup>Carbon could not be analyzed because the grains were coated with this element. <sup>b</sup>Residual between fit and experimental data:  $NSS = \sum [k^3 \chi(k) - k^3 \chi_{fit}(k)]^2 / \sum [k^3 \chi(k)]^2 \times 100$ . <sup>c</sup>Ca and Zn concentrations given in Table I. <sup>d</sup>Simulations shown in Figure 9.

Zn, multiplicity of Zn-binding environments, and presence of light elements (C, Si, and P) in the second coordination sphere of Zn in these species. Despite these difficulties, their occurrence suggested by EXAFS data is supported by the detection of Si and P by SEM-EDX and by the fact that tobacco trichomes excrete organic compounds.

## DISCUSSION

The positive effect of Ca on metal tolerance shown here has been observed in other plant species (Chen et al., 2000; Samecka-Cymerman and Kempers, 2001). Generally, this effect is attributed to a modification of the speciation of the metal in the nutrient solution and its competition with Ca for the plant uptake. In this study, increasing the Ca supply inhibited the Zn uptake after 24 h but not after 2 and 5 weeks of exposure. Consequently, the positive effect of Ca on Zn tolerance results from a cooperative and not an inhibition mechanism between the two elements. Ca

and Zn supplements increased the density of the trichomes and led to the production of Ca/Zn-containing grains (Table III; Fig. 2, C and F), suggesting that this excretion is a way to eliminate the excess of Zn from the plant tissues.

The mineralogical analysis of the grains showed that they contained calcium carbonates (primarily Zn-substituted calcite and, secondarily, vaterite and aragonite) and CaC<sub>2</sub>O<sub>4</sub> mono- and dihydrate. CaC<sub>2</sub>O<sub>4</sub> is a rather common mineral in higher plants. In tobacco, it has been found in the vacuoles of specialized leaf cells, called idioblasts (Bouropoulos et al., 2001), and its presence in the trichome cells has been suggested (Wagner et al., 2004). This mineral has been shown to sequester heavy metals in some higher plants (Mazen, 2004, and refs. therein) and lichens (Sarret et al., 1998, and refs. therein). This study shows that this is not the case in the grains excreted by tobacco trichomes. CaCO<sub>3</sub> is less usual in plants. Cystoliths, which are calcified bodies formed in specialized cells called lithocysts, have been described in some plants (Setoguchi et al., 1989). These structures consist predominantly of amorphous CaCO<sub>3</sub>,

along with subordinate amounts of calcite and vaterite, and their function is unclear. This study reports the formation of several types of  $\text{CaCO}_3$  by tobacco and the sequestration of Zn specifically in calcite. Other chemical forms of Zn found in the grains were Zn-organic acids, Zn-sorbed silica, and Zn-sorbed phosphate. Si is not a component of the nutrient solution. This element might come from glass vessels used to prepare the solutions. The proportion of Zn-substituted calcite relative to the other forms increased with Ca concentration in the nutrient medium.

Although the mechanism of formation of the grains remains unclear, some speculations can be offered. Considering the diameter of the grains (10–150  $\mu\text{m}$ ) and the diameter of the trichome plasmodesmata of tobacco (Waigmann et al., 1997), they are obviously formed externally. However, Zn and Ca are bioaccumulated within the trichomes before their exudation as shown by  $\mu\text{XRF}$ , and more precisely in the top cells for Zn, as shown by CLSM (Ca not studied by CLSM). The fact that each grain is heterogeneous in chemical composition and consists in an aggregate of submicrometer-sized particles might be due to an excretion of Ca, Zn, and the other elements in liquid form, followed by precipitation in contact with air. The predominance of calcite relative to the other  $\text{CaCO}_3$  polymorphs further supports this hypothesis. Indeed, in a supersaturated solution of  $\text{Ca}^{2+}$  and  $\text{CO}_3^{2-}$ , amorphous  $\text{CaCO}_3$  precipitates first, then transforms to vaterite, and finally to calcite, which is the most thermodynamically stable  $\text{CaCO}_3$  polymorph (Ogino et al., 1990). In the presence of  $\text{Mg}^{2+}$ , the formation of aragonite is favored at the expense of calcite. Therefore, following the definition of Lowenstam and Weiner (1989), the crystallization process seems to be biologically induced rather than biologically controlled.

In the perspective of metal exposure through smoking, an enhanced excretion of metal-containing grains during the plant growth and the removal of the grains during the cigarette manufacturing process might help to decrease the Zn and Cd content in the tobacco products. Studies on the genetics of trichome differentiation and excretion (Hallahan et al., 2000; Wagner et al., 2004) should contribute to better understand, and possibly enhance, metal excretion through the trichomes. In contrast, in the perspective of phytoextraction, the production and the release of metal-containing grains to the soil should be avoided to optimize the metal content in the harvested shoots. In this study, Zn sequestered amount in the grains of in vitro plants represented 9.2% and 16.9% in Zn- and Zn + Ca-treated plants, respectively, as estimated from the number and chemical composition of the grains. To estimate more realistically the proportion of excreted Zn, one should monitor the production and composition of the grains during the whole growth period and consider the total content of Zn in leaf at the time of the harvest.

Finally, this study illustrates the potential of micro-focused x-ray techniques in the fields of biominerali-

zation and bioremediation. When combined with molecular biology and biochemical tools, these techniques should provide key information on the strategies developed by plants to cope with metal toxicity and maintain metals homeostasis.

## MATERIALS AND METHODS

### Plant Cultures

The culture conditions and the experimental techniques are listed in Table I. For the hydroponic cultures, seeds were germinated on solid medium-filled PCR tubes and transferred after 3 weeks to 1.5-L pots (three plants per pot) filled with one-tenth-strength Hoagland medium. Fe was supplied as *N,N*-di-(2-hydroxybenzoyl)-ethylendiamine *N,N'*-di-acetic acid (5  $\mu\text{M}$ ; Weber et al., 2004). To avoid insect attack and dust contamination, plants were grown at 22°C in a closed culture box in a growth chamber with 16-h-light/8-h-dark cycle. After 3 weeks in the Hoagland medium, plants were maintained in this medium containing 0.08  $\mu\text{M}$   $\text{ZnSO}_4$  and 0.28 mM  $\text{CaCl}_2$  (control medium) or transferred to a medium containing 0.25 mM  $\text{ZnSO}_4$  and 0.28 mM  $\text{CaCl}_2$  (Zn treatment) or 0.25 mM  $\text{ZnSO}_4$  and 3.28 mM  $\text{CaCl}_2$  (Zn + Ca treatment; Table I). After 2 or 5 weeks, shoots and roots were harvested separately. The height of the shoots and the root length were measured. Aliquots of shoots were freeze-dried, weighted, and digested in 10 mL of 60% nitric acid by a microwave system ( $\mu\text{PREP-A}$ ; MLS GmbH) applying the following gradient program: 2.5 min, 700 W, 75°C, 15 bar; 8 min, 500 W, 130°C, 25 bar; 12 min, 1,000 W, 200°C, 45 bar; and 24 min, 1,000 W, 200°C, 45 bar. Zn concentrations in the digests were measured by inductively coupled plasma-atomic emission spectrometry with a Perkin-Elmer OPTIMA 300DV. Chlorophyll was extracted with 80% acetone and measured spectrophotometrically as described by Delfine et al. (1999). Each analysis was done on three replicates.

For the short-term (24-h) exposure, plants were precultured in the Hoagland medium for 5 weeks and transferred to the control, Zn, and Zn + Ca media (Table I). After 24 h, plants were harvested and analyzed as describe above.

For in vitro culture, seed-derived plants at about 5-cm height were transferred in 300-mL glass culture bottles containing one-third-strength Murashige and Skoog medium solidified with 0.7% agar and 1% Suc and exposed to 0.03 mM  $\text{ZnSO}_4$  and 3 mM  $\text{CaCl}_2$  (in vitro-control), 1 mM  $\text{ZnSO}_4$  and 3 mM  $\text{CaCl}_2$  (in vitro-Zn treatment), and 1 mM  $\text{ZnSO}_4$  and 30 mM Ca (in vitro-Zn + Ca treatment; Table I). Plants were cultivated in a growth room at 25°C under a 16-h photoperiod (35  $\mu\text{mol m}^{-2} \text{s}^{-1}$  white fluorescent tubes). Trichome densities were determined under VP-SEM (S-3500N; Hitachi) by counting the short and long trichomes on the third leaf from the top and dividing these numbers by the leaf area. To collect the grains, plants were plunged in pure water in 50-mL tubes and vortexed for a few seconds. The supernatant was carefully removed, and the grains were collected at the bottom with a pipette. Another isolation procedure was tested: grains were carefully collected using toothpicks under a stereomicroscope (Olympus SZX11-ST). Thereafter, grains were dried in vacuo (Speed Vac SC100; Savant Instruments), counted under VP-SEM (S-3500N; Hitachi), and analyzed chemically by EDX. To test the solubility of isolated grains, solutions with wide range of pH (2.0, 3.0, 4.0, 5.0, 7.0, 9.0, and 12.5) were prepared by adjusting the pH of ultrapure water with HCl or NaOH. Isolated grains were put in water drops on the slide glass and then observed the time-lapse solubility under light microscope.

Also, ex vitro hydroponic culture of tobacco plants was undertaken to check that the production of Ca/Zn-containing grains was not an artifact of in vitro conditions and to obtain grains for morphological, mineralogical, and spectroscopic characterization. After 5 weeks of hydroponic culture in the control, Zn, Zn + Ca, and Ca media (Table I), grains were collected using the water extraction procedure and kept under dry atmosphere prior to analyses. Leaf segments were also harvested and directly observed under VP-SEM-EDX or plunged in liquid nitrogen and freeze-dried for elemental mapping by  $\mu\text{XRF}$ .

### VP-SEM-EDX and SEM-EDX

Hydrated leaves and isolated grains from the in vitro and hydroponic cultures were glued on an aluminum stub, then mounted in a chamber stage after cooling to  $-20^\circ\text{C}$  and observed by VP-SEM-EDX using a Hitachi S-3500N fitted with a Horiba EMAX-7000 x-ray detector (Kuboki and Wada, 1995). The chamber pressure was 30 Pa and the accelerating voltage 15 kV. Isolated grains

from the hydroponic cultures were also analyzed by SEM-EDX using a JEOL JSM 840A microscope fitted with a Kevex Si (Li) x-ray detector. The grains were attached on a C stub with C tape and coated with C. The analyses were performed under vacuum at an accelerating voltage of 15 kV.

## CLSM

For visualization of intracellular Zn, leaf segments of plants grown in hydropony in 0.25 mM Zn + 0.28 mM Ca control (Zn treatment) and 0.08  $\mu$ M Zn + 0.28 mM Ca (control) for 2 weeks were immersed in 1  $\times$  PBS buffer (137 mM NaCl, 2.68 mM KCl, 8.1 mM Na<sub>2</sub>HPO<sub>4</sub>, 1.47 mM KH<sub>2</sub>PO<sub>4</sub>, pH 7.4) containing 25  $\mu$ M Zinquin ethyl ester ([ethyl (2-methyl-8-*p*-toluenesulphonamido-6-quinolyloxy) acetate]; Biotium) for 1 h at 25°C. Leaf segments were washed once with PBS buffer and mounted on glass slides and examined with a CLSM system (LSM510 META NLO; Carl Zeiss) with Plan-Neofluar 10  $\times$  (0.3 NA) or 20  $\times$  (0.5 NA) water-immersion lens. Zinquin fluorescence was determined at an excitation wavelength of 368 nm with an UV Ar laser (80 mW) at an emission wavelength of 490 nm. Confocal fluorescence and concurrent differential interference contrast images were taken, and digital images were processed using AxioCam HR with LSM 5 images software.

## $\mu$ XRF, $\mu$ XRD, and $\mu$ EXAFS

The experiments were performed on beamline 10.3.2 of the Advanced Light Source, Berkeley, CA (Marcus et al., 2004). For the  $\mu$ XRF and  $\mu$ EXAFS measurements, the beam was focused down to 5  $\times$  5  $\mu$ m and the x-ray fluorescence was measured with a seven-element Ge detector. For the  $\mu$ XRD measurements, the diffraction patterns were recorded with a 1,024  $\times$  1,024 pixels CCD camera at 17 keV incident x-ray energy with a 16  $\times$  7  $\mu$ m<sup>2</sup> beam size. Isolated tobacco grains were mounted at the top of a glass capillary (0.2 mm in diameter), and the capillary fixed on a motorized x-y-z stage. The grains were cooled to 150 K with a Cryostream cooler (Oxford 611) during measurements to minimize any potential beam damage. First, a  $\mu$ XRD pattern of the whole grain was recorded by scanning it under the beam while acquiring the data. Then, a point  $\mu$ XRD pattern, a  $\mu$ XRF spectrum, and a Zn K-edge EXAFS spectrum (if Zn present) were recorded successively on the Ca- and Zn-richest spots.  $\mu$ XRF elemental maps from the freeze-dried leaf segments were recorded at room temperature in mounting the sample directly on the x-y-z stage.

## XRD and EXAFS Data Treatment

The two-dimensional XRD patterns were calibrated using an alumina standard and integrated to one-dimensional patterns for peak assignment with the JCPDS database (<http://www.icdd.com>). The stoichiometry of the Mg-, Mn-, and Zn-substituted crystals was estimated by refining the unit cell parameters *a* and *c* over the [10–33]  $^{\circ}$   $2\theta$  angular range ([1.3–4.0] Å interval) using the Ufit software (M. Evain, 1992), and then by applying the Vegard law (West, 1984) using calcite and magnesite (MgCO<sub>3</sub>) as end-members for the Ca-Mg solid solution; calcite and rhodocrosite (MnCO<sub>3</sub>) as end-members for the Ca-Mn solid solution; and calcite and smithsonite (ZnCO<sub>3</sub>) as end-members for the Ca-Zn solid solution.

EXAFS spectra were extracted using the standard procedure and then simulated by linear combinations of reference spectra from an extended spectral library (Sarret et al., 2004; Guiné et al., 2006). The spectrum for Zn-substituted calcite was provided by R.J. Reeder (Reeder et al., 1999; Elzinga and Reeder, 2002). Zn-sorbed silica was prepared by adding 40 mg of Zn(NO<sub>3</sub>)<sub>2</sub>  $\cdot$  4 H<sub>2</sub>O (2.55 mM Zn) to a suspension containing 0.5 g of silica (aerosil 200; Degussa) pre-equilibrated at pH 6.0, stirring the suspension for 2 h at pH 6.0, centrifugating it, and freeze-drying the solid phase. The final Zn content was 2 wt %. The Zn-humic acid and Zn-reacted hydroxylapatite references were described previously (Sarret et al., 1997; Panfili et al., 2005).

## ACKNOWLEDGMENTS

We thank Delphine Tisserand and Martine Lanson (Laboratoire de Géophysique Interne et Tectonophysique, France), Sébastien Pairis (Laboratoire de Cristallographie, France), Sylvia Krüger (Leibniz-Institut für Pflanzenbiochemie, Germany), and Jeong-Yeon Han (Kangwon National University, Korea) for their technical assistance. VP-SEM-EDX and CLSM analyses were performed at Korea Basic Science Institute, Chunchon, South Korea. We

acknowledge R.J. Reeder for sharing the Zn-calcite EXAFS spectrum, and Prof. Dierk Scheel and Dr. Dieter Neumann (Leibniz-Institut für Pflanzenbiochemie) for fruitful discussions.

Received April 28, 2006; revised April 28, 2006; accepted May 22, 2006; published May 26, 2006.

## LITERATURE CITED

- Ager FJ, Ynsa MD, Domínguez-Solís JR, López-Martín MC, Gotor C, Romero LC (2003) Nuclear micro-probe analysis of *Arabidopsis thaliana* leaves. *Nucl Inst Meth Phys Res B* **210**: 401–406
- Arnott HJ, Pautard FGE (1970) Calcification in plants. In H Schraer, ed, *Biological Calcification: Cellular and Molecular Aspects*. Appleton-Century-Crofts, New York, pp 375–446
- Bouropoulos N, Weiner S, Addadi L (2001) Calcium oxalate crystals in tomato and tobacco plants: morphology and *in vitro* interactions of crystal-associated macromolecules. *Chem Eur J* **7**: 1881–1888
- Bringezu K, Lichtenberger O, Leopold I, Neumann D (1999) Heavy metal tolerance of *Silene vulgaris*. *J Plant Physiol* **154**: 536–546
- Broadhurst CL, Chaney RL, Angle JS, Maugel TK, Erbe EF, Murphy CA (2004) Simultaneous hyperaccumulation of nickel, manganese, and calcium in *Alyssum* leaf trichomes. *Environ Sci Technol* **38**: 5797–5802
- Chen ZS, Lee GJ, Liu JC (2000) The effects of chemical remediation treatments on the extractability and speciation of cadmium and lead in contamination soils. *Chemosphere* **41**: 235–242
- Choi YE, Harada E (2005) Roles of calcium and cadmium on Cd-containing intra- and extracellular formation of Ca crystals in tobacco. *J Plant Biol* **48**: 113–119
- Choi YE, Harada E, Kim GH, Yoon ES, Sano H (2004) Distribution of elements on tobacco trichomes and leaves under cadmium and sodium stresses. *J Plant Biol* **47**: 75–82
- Choi YE, Harada E, Wada M, Tsuboi H, Morita Y, Kusano T, Sano H (2001) Detoxification of cadmium in tobacco plants: formation and active excretion of crystals containing cadmium and calcium through trichomes. *Planta* **213**: 45–50
- Coyle P, Zalewski PD, Philcox JC, Forbes IJ, Ward AD, Lincoln SE, Mahadevan I, Rofe AM (1994) Measurement of zinc in hepatocytes by using a fluorescent probe, Zinquin: relationship to metallothionein and intracellular zinc. *Biochem J* **303**: 781–786
- Delfine S, Alvino A, Villiani MC, Loreto F (1999) Restrictions to carbon dioxide conductance and photosynthesis in spinach leaves recovering from salt stress. *Plant Physiol* **119**: 1101–1106
- deSilva DLR, Hetherington AM, Mansfield TA (1996) Where does all the calcium go? Evidence of an important regulatory role for trichomes in two calcicoles. *Plant Cell Environ* **19**: 880–886
- Domínguez-Solís JR, López-Martín MC, Ager FJ, Ynsa MD, Romero LC, Gotor C (2004) Increased cysteine availability is essential for cadmium tolerance and accumulation in *Arabidopsis thaliana*. *Plant Biotechnol J* **2**: 469–476
- Elzinga EJ, Reeder RJ (2002) X-ray absorption spectroscopy study of Cu<sup>2+</sup> and Zn<sup>2+</sup> adsorption complexes at the calcite surface: implications for site-specific metal incorporation preferences during calcite crystal growth. *Geochim Cosmochim Acta* **66**: 3943–3954
- Fleisher RL, Parungo FP (1974) Aerosol particles on tobacco trichomes. *Nature* **250**: 158–159
- Goldstein JI, Newbury DE, Echlin P, Joy DC, Fiori C, Lifshin E (1981) *Scanning Electron Microscopy and X-Ray Microanalysis*. Plenum Press, New York
- Guiné V, Spadini L, Sarret G, Muris M, Delolme C, Gaudet J, Martins J (2006) Zinc sorption to three gram-negative bacteria: combined titration, modeling and EXAFS study. *Environ Sci Technol* **40**: 1806–1813
- Hallahan D, Gray J, Callow J, editors (2000) *Advances in Botanical Research: Plant Trichomes*. Academic Press, London
- Iwasaki K, Matsumura A (1999) Effect of silicon on alleviation of manganese toxicity in pumpkin (*Cucurbita moschata* Duch cv. Shintosa). *Soil Sci Plant Nutr* **45**: 909–920
- Kuboki K, Wada M (1995) The variable pressure SEM with the cooling stage. *Hitachi Instrum News* **27**: 20–25
- Küpper H, Kroneck PMH (2005) Heavy metal uptake by plants and cyanobacteria. In A Sigel, H Sigel, R Sigel, eds, *Metal Ions In Biological Systems*, Vol 44. Marcel Dekker, New York, pp 92–142

- Küpper H, Lombi E, Zhao FJ, McGrath SP** (2000) Cellular compartmentation of cadmium and zinc in relation to other elements in the hyperaccumulator *Arabidopsis halleri*. *Planta* **212**: 75–84
- Lavid N, Barkay Z, Tel-Or E** (2001) Accumulation of heavy metals in epidermal glands of the waterlily (Nymphaeaceae). *Planta* **212**: 313–322
- Lowenstam H, Weiner S** (1989) *On Biomineralization*. Oxford University Press, New York, Oxford
- Lugon-Moulin N, Zhang M, Gadani F, Rossi L, Koller D, Krauss M, Wagner GJ** (2004) Critical review of the science and options for reducing cadmium in tobacco (*Nicotiana tabacum* L.) and other plants. *Adv Agron* **83**: 111–180
- MacFarlane GR, Burchett M** (1999) Zinc distribution and excretion in the leaves of the grey mangrove, *Avicennia marina* (Forsk.) Vierh. *Environ Exp Bot* **41**: 167–175
- Manceau A, Marcus MA, Tamura N** (2002) Quantitative speciation of heavy metals in soils and sediments by synchrotron X-ray techniques. In P Fenter, M Rivers, N Sturchio, S Sutton, eds, *Applications of Synchrotron Radiation in Low-Temperature Geochemistry and Environmental Science*, Vol 49. Reviews in Mineralogy and Geochemistry. Mineralogical Society of America, Washington, DC, pp 341–428
- Marcus MA, MacDowell AA, Celestre R, Manceau A, Miller T, Padmore HA, Sublett RE** (2004) Beamline 10.3.2 at ALS: a hard X-ray microprobe for environmental and materials sciences. *J Synchrotron Radiat* **11**: 239–247
- Mazen AMA** (2004) Calcium oxalate deposits in leaves of *Corchorus olitorius* as related to accumulation of toxic metals. *Russ J Plant Physiol* **51**: 281–285
- Neumann D, zur Nieden U, Lichtenberger O, Leopold I** (1995) How does *Armeria maritima* tolerate high heavy metal concentrations? *J Plant Physiol* **146**: 704–717
- Ogino T, Suzuki T, Sawada K** (1990) The rate and mechanism of polymorphic transformation of calcium carbonate in water. *J Cryst Growth* **100**: 159–167
- Panfili F, Manceau A, Sarret G, Spadini L, Kirpichtchikova T, Bert V, Laboudigue A, Marcus MA, Ahamdach N, Libert MF** (2005) The effect of phytostabilization on Zn speciation in a dredged contaminated sediment using scanning electron microscopy, X-ray fluorescence, EXAFS spectroscopy and principal components analysis. *Geochim Cosmochim Acta* **69**: 2265–2284
- Reeder RJ, Lamble GM, Northrup PA** (1999) XAFS study of the coordination and local relaxation around  $\text{Co}^{2+}$ ,  $\text{Zn}^{2+}$ ,  $\text{Pb}^{2+}$  and  $\text{Ba}^{2+}$  trace elements in calcite. *Am Mineral* **84**: 1049–1060
- Rodriguez E, Healey PL, Mehta I, editors** (1983) *Biology and Chemistry of Plant Trichomes*. Plenum Press, New York
- Salt DE, Prince RC, Pickering IJ, Raskin I** (1995) Mechanisms of cadmium mobility and accumulation in Indian mustard. *Plant Physiol* **109**: 1427–1433
- Samecka-Cymerman A, Kempers AJ** (2001) Concentration of heavy metals and plant nutrients in water, sediments and aquatic macrophytes of anthropogenic lakes (former open cut brown coal mines) differing in stage of acidification. *Sci Total Environ* **281**: 87–98
- Sarret G, Balesdent J, Bouziri L, Garnier JM, Marcus MA, Geoffroy N, Panfili F, Manceau A** (2004) Zn speciation in the organic horizon of a contaminated soil by micro X-ray fluorescence, micro and powder EXAFS spectroscopy and isotopic dilution. *Environ Sci Technol* **38**: 2792–2801
- Sarret G, Manceau A, Cuny D, Van Haluwyn C, Deruelle S, Hazemann JL, Soldo Y, Eybert-Bérard L, Menthonnex JJ** (1998) Mechanism of lichen resistance to metallic pollution. *Environ Sci Technol* **32**: 3325–3330
- Sarret G, Manceau A, Hazemann JL, Gomez A, Mench M** (1997) EXAFS study of the nature of zinc complexation sites in humic substances as a function of Zn concentration. *J Phys IV* **7**: 799–802
- Sarret G, Saumitou-Laprade P, Bert V, Proux O, Hazemann JL, Traverse A, Marcus MA, Manceau A** (2002) Forms of zinc accumulated in the hyperaccumulator *Arabidopsis halleri*. *Plant Physiol* **130**: 1815–1826
- Setoguchi H, Okazaki M, Suga S** (1989) Calcification in higher plants with special reference to cystoliths. In R Crick, ed, *Origin, Evolution, and Modern Aspects of Biomineralization in Plants and Animals*. Plenum Press, New York, pp 409–418
- Shannon RD** (1976) Revised effective ionic radius and systematic studies of interatomic distances in halides and chalcogenides. *Acta Crystallogr A* **32**: 751–767
- Shepherd RW, Bass WT, Houtz RL, Wagner GJ** (2005) Phylloplanins of tobacco are defensive proteins deployed on aerial surface by short glandular trichomes. *Plant Cell* **17**: 1851–1861
- Song W-Y, Sohn EJ, Martinoia E, Lee YJ, Yang Y-Y, Jasinski M, Forestier C, Hwang I, Lee Y** (2003) Engineering tolerance and accumulation of lead and cadmium in transgenic plants. *Nat Biotechnol* **21**: 914–919
- Stephens WE, Calter A, Newton J** (2005) Source and health implications of high toxic metal concentrations in illicit tobacco products. *Environ Sci Technol* **39**: 479–488
- Wagner GJ, Wang E, Shepherd RW** (2004) New approaches for studying and exploiting an old protuberance, the plant trichome. *Ann Bot (Lond)* **93**: 3–11
- Waignann E, Turner A, Peart J, Roberts K, Zambryski P** (1997) Ultrastructural analysis of leaf trichome plasmodesmata reveals major differences from mesophyll plasmodesmata. *Planta* **203**: 75–84
- Weber M, Harada E, Vess C, von Roepenack-Lahaye E, Clemens S** (2004) Comparative microarray analysis of *Arabidopsis thaliana* and *Arabidopsis halleri* roots identifies nicotianamine synthase, a ZIP transporter and other genes as metal hyperaccumulation factors. *Plant J* **37**: 269–281
- West A** (1984) *Solid State Chemistry and Its Applications*. Wiley, New York
- Zhao F, Lombi E, Breedon T, McGrath SP** (2000) Zinc hyperaccumulation and cellular distribution in *Arabidopsis halleri*. *Plant Cell Environ* **23**: 507–514